# Bottom dissipation of subinertial currents at the Atlantic zonal boundaries

C. J. Wright,[1] R. B. Scott,[1,2] B. K. Arbic,[3] and D. F. Furnival[1]

Received 20 October 2011; revised 14 February 2012; accepted 14 February 2012; published 31 March 2012.

[1] Estimates of the dissipation of subinertial currents due to bottom boundary layer drag at the eastern and western boundaries of the North Atlantic ocean, between 15 N and 60 N, are computed using data from the world's largest archive of ocean current meter time series. We show from these data that a significant proportion of such loss in this region is due to dissipation at the western boundary ocean floor via quadratic bottom boundary layer drag, with an estimated 40–60% (31–47 GW) of the wind input power across the whole basin dissipated by this method. We further show that the majority of this dissipation occurs at shallow depths, <500 m; this has significant implications for the power available for abyssal mixing.

**Citation:** Wright, C. J., R. B. Scott, B. K. Arbic, and D. F. Furnival (2012), Bottom dissipation of subinertial currents at the Atlantic zonal boundaries, *J. Geophys. Res.*, *117*, C03049, doi:10.1029/2011JC007702.

## 1. Introduction

[2] The majority of the mechanical energy in the deep ocean is carried by subinertial currents with horizontal length scales of at least tens of kilometers and timescales of multiple days. The mechanisms by which this energy is dissipated, however, are poorly understood [*Ferrari and Wunsch*, 2009; *Wunsch and Ferrari*, 2004]. This has significance for the general oceanic circulation. A better understanding of the underlying mechanisms would allow us to locate mixing processes within the vertical water column, providing an important constraint on the meridional overturning circulation [*Munk and Wunsch*, 1998].

[3] The main source of energy for these currents is believed to be the time mean winds, but the amount of forcing of available potential energy and the inflow of energy at the lateral boundaries remains unquantified [*Wunsch and Ferrari*, 2004]; consequently, we assess dissipation in the context of the wind-forcing, which is well-known and well-constrained [*Wunsch*, 1998; *Scott*, 1999a, 1999b; *Hughes and Wilson*, 2008; *Scott and Xu*, 2009]. Recent studies [*Scott et al.*, 2011] have shown that dissipation in the southern hemisphere occurs primarily through topographic lee wave generation, but this is a comparatively small effect in the northern hemisphere; this lee wave generation dissipates only around 10% (8.1 GW) of the wind power input to the North Atlantic.

[4] Several mechanisms have been suggested for the removal of this energy from the oceans, which can be divided broadly into two main categories: instability and wave processes acting in the interior of the water column [e.g., *Bühler and McIntyre*, 2005; *Molemaker et al.*, 2005; *Zhai et al.*, 2010] and bottom boundary layer (BBL) drag processes [e.g., *Weatherly*, 1984; *Sen et al.*, 2008; *Arbic et al.*, 2009]. Suppression by the surface winds can also be included as a third category [*Scott and Xu*, 2009; *Zhai and Greatbatch*, 2007], but is in practice already accounted for in the net input energy from the wind. This net input energy can be calculated using the method of *Scott and Xu* [2009] as around 80 GW for the North Atlantic basin as a whole.

[5] It has recently been shown that the removal of this energy in the northern hemisphere takes place primarily at the western boundary. Eddies propagate westward at the speed of Rossby waves [*Chelton et al.*, 2007; *Kanzow et al.*, 2009]leading to heightened eddy kinetic energy levels [*Kanzow et al.*, 2009; *Shum et al.*, 1990] and resulting dissipation [*Arbic et al.*, 2009; *Zhai et al.*, 2010] at the boundary, which is then lost to the system [*Wunsch and Ferrari*, 2004]. *Zhai et al.* [2010], using a combination of models, satellite altimetry, and climatological hydrographic data, estimate a sink ∼22–39 GW for the Atlantic north of $\phi = 10^{\circ}$ due to a fluxof mechanical energy into the western boundary region, and speculate that this is due to excitation of turbulence in the interior of the water column, which would potentially make this turbulence available to drive abyssal mixing. However, there are alternative mechanisms which may better explain this loss. *Arbic et al.* [2009], using the Parallel Ocean Program model, estimated a quadratic BBL dissipation sink of 28–69 GW in the shallow (<1000 m) North Atlantic and 48–120 GW in the North Atlantic at all depths, with a large proportion of this in the western boundary. These dissipation rates are large enough to account for the flux of mechanical energy into the western boundary layer estimated by *Zhai et al.* [2010] and suggest that this is an important contributing mechanism. If so, this would leave little if any of the 80 GW of the North Atlantic wind power input available to drive abyssal mixing in the important western boundary region [*Scott and Marotzke*, 2002].

[1]Laboratoire de Physique des Océans, Université de Bretagne Occidental, Brest, France.
[2]UTIG, University of Texas at Austin, Austin, Texas, USA.
[3]Department of Geological Sciences, University of Michigan, Ann Arbor, Michigan, USA.


0148-0227/12/2011JC007702

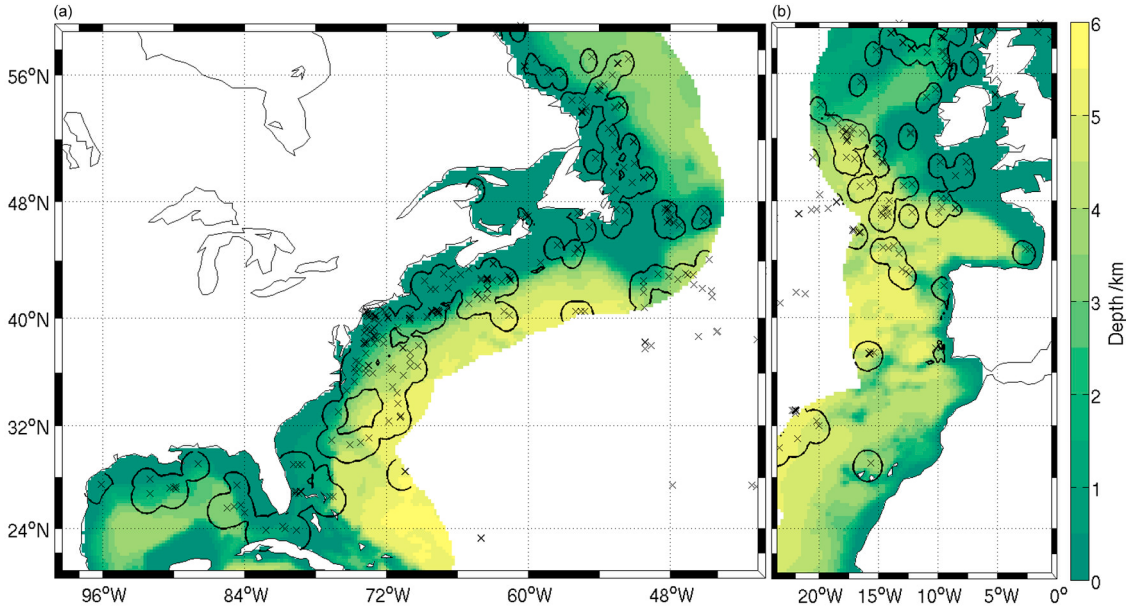


**Figure 1.** Bottom topography of the North Atlantic basin for the two boundary regions. Current meter locations considered in our analysis are highlighted by black crosses. The solid contours enclose the regions in which the nearest current meter is within a single decorrelation scale.

[6] By using a collection of ocean current time series derived from the oceanographic research programmes of multiple countries, we are able to experimentally quantify the energy lost due to dissipation of subinertial currents via quadratic BBL drag ('BBL dissipation') at the western boundary of the North Atlantic, and to contrast this with the equivalent values for the eastern boundary and with the results of previous studies.

## 2. Methods

### 2.1. Time Series Data

[7] Our time series data are derived from the Global MultiArchive Current Meter Database (GMACMD) [*Scott et al.*, 2010, 2011]. This is a global collection of (at time of writing) approximately 47,000 physical oceanographic time series, primarily derived from ocean current meters, converted into a standard format.

[8] The current meters used for our analysis are those which fall within the geographic regions outlined below and within the bottom 10% of the ocean. Shelf regions, defined as those with a depth less than 100 m are excluded, as are current meters within 10 m of the ocean bottom. Meters with less than 30 days of data are excluded from our analysis; the bulk of time series are between six months and a year in length, with the longest lasting for slightly over three years. Many current meter moorings hold multiple meters at different depths; where this is the case, only the deepest current meter is considered. Six extreme-outliers, lying more than 5 standard deviations above the overall mean for both regions, have also been excluded from our analysis. All velocity time series used have been regularized to a common three-hour time step between measurements; series with either an irregular time step or a time step shorter than this have been averaged to this value, while series with a longer time step have been discarded.

### 2.2. Regions

[9] We define the eastern and western boundaries as the region within 700 km of the shoreline between 15 N and 60 N; this criterion maximizes available coverage of measurements, while still including regions with a sufficient range of depths to allow assessment of the eddy dissipation as a function of depth. We assess the western and eastern boundaries separately.

[10] Allowing for these and the above considerations, 402 time series (289 on the western boundary, 113 on the eastern boundary) are used. These locations are shown as crosses on Figure 1; their highly uneven distribution should be noted. Also shown on Figure 1 are the areas enclosed within one decorrelation scale $\delta$ of these measurements (solid contours; see below). Currents within $\delta \leq 1$ are assumed to be well-correlated with the values at the measurement location. Around 26% of the western and 20% of the eastern boundary regions are within $\delta \leq 1$ of our measurements (see Table 1).

[11] The measurements used may exhibit a bias in their measured currents, and hence their BBL drag, due to their selection as places of interest for current measurements [*Sen et al.*, 2008; *Holloway et al.*, 2011]; accordingly, the extrapolation beyond the directly-measured region is uncertain. Estimates in section 4.2 suggest a potential negative bias in BBL dissipation due to this extrapolation of 5–20% on the eastern boundary and a potential positive bias of 0–50% on the western boundary. Nevertheless, the values for $\delta \leq 1$ can be considered to be accurate, and hence will form a sensible lower bound on the BBL dissipation.

### 2.3. Decorrelation Scales

[12] We define the longitudinal and latitudinal decorrelation scales $\delta_\theta$ and $\delta_\phi$ as [*Ducet et al.*, 2000]

$$\delta_\theta = \delta_\phi = 50 + 250\left(\frac{900}{900 + 2\phi^2}\right)\text{km}, \qquad (1)$$

**Table 1.** Key Data for the Two Regions Considered[a]

| | | $\delta \le 1$ | | | All Locations | | |
|---|---|---|---|---|---|---|---|
| Region | Time Series | $D_e$ | A | Percent | $D_e$ | A | Percent |
| Western | 289 | 15.0 | 2400 | 32.1 | 47.0 | 6880 | 100 |
| Eastern | 113 | 2.5 | 790 | 18.1 | 9.3 | 4320 | 100 |

[a]'$D_e$' indicates the total BBL dissipation measured in GW, 'A' indicates the total area in thousands of square kilometers, and 'Percent' indicates the proportion of the total area. Results are shown for distances within 1 decorrelation scale $\delta$ of a current meter and extrapolated over the whole region.

where $\phi$ is in degrees, and the vertical decorrelation scale as

$$\delta_z = \left(\frac{f}{N}\right)\left(\frac{2}{\delta_\theta^{-1} + \delta_\phi^{-1}}\right), \tag{2}$$

where $N$ is the Brunt-Väisälä frequency and $f$ the Coriolis parameter. The calculations for $\delta_\theta$ and $\delta_\phi$ are the same in the cases we consider in this study, but differ at latitudes <14°; we retain the two terms separately here to agree with *Ducet et al.* [2000]. Values of $N$ are determined from the WOA2009 seasonal temperature and salinity climatology using equation 3.71 of *Gill* [1982] and averaged over the seasons, omitting negative values. The values for $\delta_\theta$, $\delta_\phi$ and $\delta_z$ are then summed in quadrature to give an overall measure for decorrelation length $\delta$ at a given point

$$\delta = \sqrt{\left(\frac{\Delta\phi}{\delta_\phi}\right)^2 + \left(\frac{\Delta\theta}{\delta_\theta}\right)^2 + \left(\frac{\Delta z}{\delta_z}\right)^2}, \tag{3}$$

where $\Delta\phi$ represents the latitudinal distance between the point and the meter in the same units as $\delta_\phi$, etc. $\delta$ is hence dimensionless.

### 2.4. BBL Dissipation

[13] BBL dissipation results from quadratic BBL momentum drag, parameterized as a term

$$\frac{\rho c_d \sqrt{u^2 + v^2}\ \mathbf{u}}{H}, \tag{4}$$

where $\rho = 1035$ kg m$^{-3}$ is the mean density seawater density, $c_d = 0.0025$ is the quadratic bottom drag coefficient, $\mathbf{u} = (u, v)$ is the background flow velocity above the BBL, and $H$ is the BBL thickness. Taking the inner product with $\mathbf{u}$ and integrating over $H$, we obtain the standard formula for quadratic BBL dissipation

$$\rho c_d |\mathbf{u}|^3. \tag{5}$$

To focus on the dissipation of the subinertial, essentially geostrophic, flow, $D_e$, requires some care because of the nonlinearity of the dissipation on flow velocity. The formula for $D_e$ that retains the dissipation due to interaction between high and low frequencies, is

$$D_e = \rho c_d \left\langle \sqrt{u^2 + v^2}\ \mathbf{u} \right\rangle \cdot \langle \mathbf{u} \rangle, \tag{6}$$

where $\langle x \rangle$ is the low-pass filter of time series $x$, here a Butterworth filter with 3-day cutoff. For interest we also isolated the dissipation due to interaction between high and low frequencies,

$$\rho c_d \left\langle \sqrt{u^2 + v^2}\ \mathbf{u} \right\rangle \cdot \langle \mathbf{u} \rangle - \rho c_d |\langle \mathbf{u} \rangle|^3 \tag{7}$$

and found it to generally be around 15% of the $D_e$ in shallow seas where the tides were strong, and less in the deep ocean thus justifying the omission of this component of the dissipation in previous studies [*Sen et al.*, 2008; *Arbic et al.*, 2009].

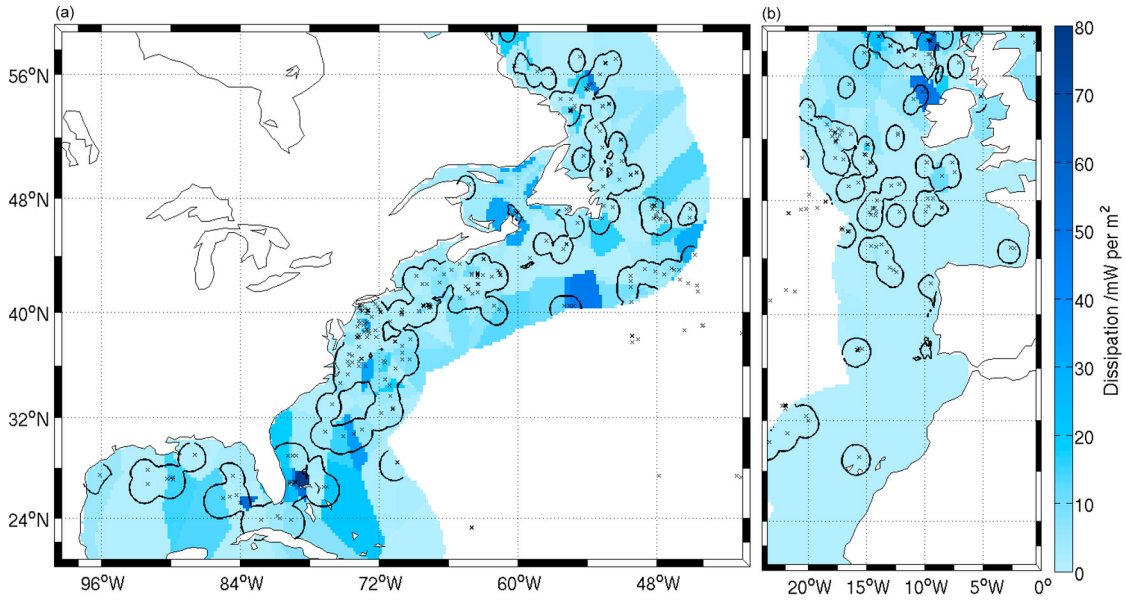


**Figure 2.** Maps showing the geographic distribution of BBL dissipation in the two boundary regions.

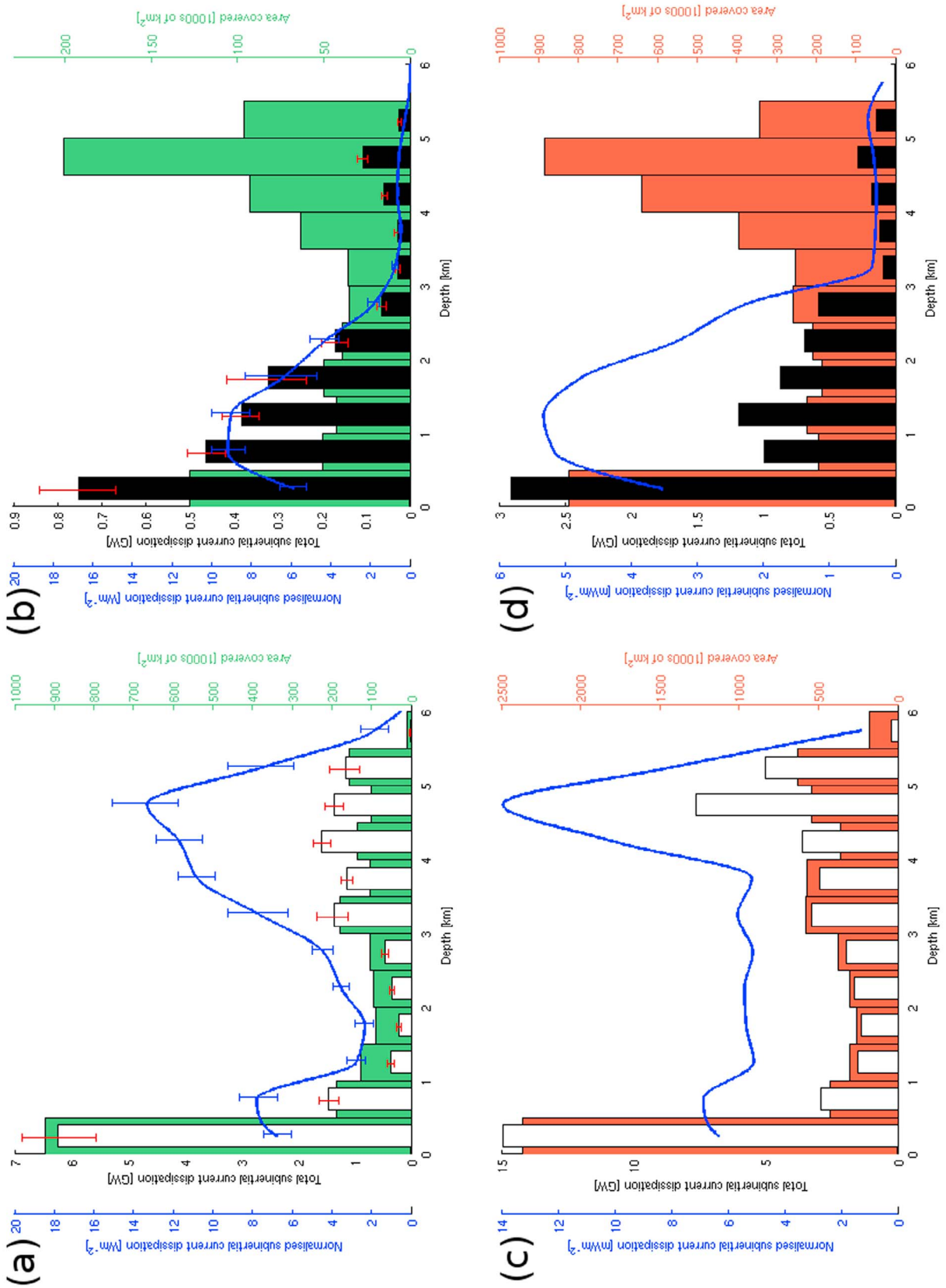
(a)
(b)
(c)
(d)
Depth [km]
Total subinertial current dissipation [GW]
Normalised subinertial current dissipation [mWm$^{-2}$]
Area covered [1000s of km$^2$]

Figure 3

### 2.5. Analysis

[14] We compute the time-mean value of $D_e$ (per unit area; $Wm^{-2}$) at each measurement location, and then extrapolate these values to cover the entire area on a regular $0.25^\circ \times 0.25^\circ$ grid. For each grid point, we assign a value of $D_e$ equal to the value of the nearest measurement, defined as that the smallest multiple of $\delta$ away. This may not be the closest measurement geographically, as the calculation of $\delta$ is $z$-weighted; accordingly, a measurement at a similar depth may be selected in preference to one geographically closer but at a very different depth.

## 3. Results

### 3.1. Geographic

[15] Figure 2 shows estimates for the BBL dissipation. The first key result observed is that estimated values are significantly lower in the eastern boundary region (Figure 2b) than in the western boundary region (Figure 2a). Values observed in the eastern boundary, with the exception of some small outlier regions around the British Isles which reach up to 50 $mWm^{-2}$, peak at $\sim$10 $mWm^{-2}$, while values on the western boundary are larger in general, with an absolute peak near Florida at $\sim$80 $mWm^{-2}$, around 25 $mWm^{-2}$ above the absolute peak on the eastern boundary. The highest values on the eastern boundary south of the English Channel reach no higher than 3 $mWm^{-2}$; in contrast, high values are observed along the entire western boundary, with particular peaks around Florida, east of the coast of Labrador, and in the Gulf Stream near $\sim$(41 N, 52 W). These peaks are consistent with the effects of the strong western boundary current.

### 3.2. By Depth

[16] Figure 3 shows the same results, divided up by $\delta$ (separate plots) and depth (horizontal axis, in 500 m bins). The wide bars show area, narrow bars total estimated BBL dissipation, and the line measured BBL dissipation per unit area $D_e$. We also obtain summed values over all depths (Table 1).

[17] Figures 3a and 3b show results for $\delta \leq 1$, i.e., the region which should be well-correlated with our measurement locations, and hence the most confident results. We observe in both regions that the highest measured values of unnormalized BBL dissipation occur in the shallowest regions, with secondary peaks at high depths. In the western boundary this secondary peak is at depths below $\sim$3 km; this is consistent with the intense and more depth-independent flow of Gulf Stream eddies observed by *Schmitz and Luyten* [1991], which presumably barotropise through nonlinear interactions. In contrast, the eastern boundary shows a much smaller secondary peak at depths below 4 km, with values otherwise declining with depth. Normalized dissipation shows high values at high depths on the western boundary, but as total area is small here compared to the shallower regions this makes a comparatively small contribution to the total. 15.0 GW is estimated for $\delta \leq 1$ on the western boundary against 2.5 GW on the eastern; while the area within $\delta \leq 1$ on the western boundary is around thrice that on the eastern, this is still a massive imbalance, consistent with the significantly greater energy loss expected at the western boundary.

[18] As discussed above, the results for $\delta \leq 1$ provide an accurate lower bound on the BBL dissipation estimates, whereas our extrapolation from this value may be positive-biased: it is hence important to note that the estimated dissipation in this third of the total western boundary area region makes up nearly 70% of Zhai et al's lower bound of 22 GW. On this boundary, around 40% of the estimated dissipation is at shallow depths, <1 km; while there is substantial dissipation per unit area in the deeper regions, the actual area at these depths is small, leading to an overall contribution of around 30% of measured BBL dissipation in the western boundary from depths >4 km. This is not the case in the eastern boundary: while dissipation declines with increasing depth, there is no single depth range which dominates in the way we see in the west.

[19] Figures 3c and 3d show extrapolated results for the entire region on both boundaries. Distributions observed are broadly similar to those measured for $\delta \leq 1$; in the eastern boundary, most BBL dissipation is in shallower regions, while in the western boundary there is a substantial secondary peak at high depth. Total BBL dissipation for the two boundary regions is again sharply different: for the all-locations case, BBL dissipation in the eastern boundary totals 9.3 GW compared to 47.0 GW for the western boundary. Given our estimated positive bias and their expected negative bias, this is comparable to the $\sim$22–39 GW estimated by *Zhai et al.* [2010] for the sink of subinertial current energy in the North Atlantic, and hence suggests that bottom boundary layer dissipation may be one of the dominant processes acting to dissipate these currents here. It also compares favorably to the results of *Arbic et al.* [2009], with the two regions totalling 56.3 GW compared to their range of 48–120 GW for whole North Atlantic basin. Again, while there is a substantial secondary peak of $D_e$, the bulk of the measured BBL dissipation is in the shallow regions, again consistent with Arbic et al. The proportion of dissipation in the extrapolated areas of the western boundary is broadly similar to that within $\delta < 1$, with around 50% at depths <1 km and around 10% at depths >4 km.

## 4. Discussion

### 4.1. Errors: Statistical

[20] For the directly-measured $\delta \leq 1$ region, a statistical bootstrapping process [*Efron*, 1979] is used. This works as follows.

[21] For each individual time series, we compute ten-day non-overlapping means of the BBL dissipation $D_e$. This criterion of ten days is determined by an analysis of the time taken for each series to auto-decorrelate: $\sim$90% of the time series auto-decorrelate within this time. We then select all grid points on our $0.25 \times 0.25$ degree grid which lie within

**Figure 3.** BBL dissipation as a function of depth. (a and b) Results for areas where $\delta \leq 1$ and (c and d) the extrapolated results for the whole region are shown; Figures 3a and 3c show the western boundary and Figures 3b and 3d show the eastern. Wide bars indicate area on the right-hand scale, narrow bars the total BBL dissipation on the inner left-hand scale, and the curve the BBL dissipation per unit area on the outer left-hand scale. Note the different scales on each figure.

$\delta \leq 1$ of a measurement location, and subdivide by depth; for each 500 m depth bin, we select all contributing time series, area-weight them appropriately, and then resample the mean of each ten-day-averaged area-weighted series one thousand times to obtain estimates of the BBL dissipation due to that series. For each of the thousand trials, we then sum over all the contributing area-weighted series, obtaining a distribution of one thousand total BBL dissipation values for each depth bin, and select the 95% confidence interval. This is indicated on Figures 3a and 3b by the whiskered lines for each dissipation bar. No uncertainty is indicated on the area bars as these values are well-known.

### 4.2. Errors: Extrapolation

[22] The bootstrapping method was not used for our extrapolation to the full area, as the effects due to statistical variability were considered to be less than the inherent uncertainty introduced to the extrapolation by the uneven distribution of the measurement locations. As such, statistically-derived uncertainties on these results would convey a false sense of the true uncertainty. Instead, to assess the biases on our extrapolation to the full area, comparisons were performed to ocean-bottom modeled currents (HYCOM) [*Chassignet et al.*, 2007] and to surface current data obtained via satellite altimetry (Collecte Localisation Satellites) [*Ducet et al.*, 2000], using the same methodology as for the current meter analyses discussed above. These data are regularly-gridded over the whole basin, and should not suffer an especial bias toward any individual region. Thus, while there may be inherent differences in the magnitudes computed via these methods, the ratio between the total values for the measured and extrapolated areas is useful as an estimate of the bias introduced by the locations of our measurements. It should be noted that the satellite data is used solely to assess a proxy to the BBL dissipation based on surface currents, not a direct estimate of the BBL dissipation itself.

[23] Each data set was interpolated to the same 0.25 $\times$ 0.25 degree grid used in our analysis, and the same spatial selection criteria (latitude and distance from coast) applied; mean dissipations for the region within $\delta \leq 1$ of a current meter and the whole region were then computed and compared. Results were computed separately for the east and west boundaries as a ratio of the mean for the whole region to the mean for the region where $\delta \leq 1$; a value less than 1 indicates that an extrapolation from $\delta \leq 1$ to the whole region will be negative-biased and vice versa.

[24] For the eastern boundary, both the model and satellite studies suggest that our results slightly underestimate the result, with ratios of 1.0 and 0.8 for the satellite and model results respectively. This implies that values on the eastern boundary may be up to 20% higher than we estimate. For the western boundary, the results are slightly more divergent. The model gives a ratio of 1.0, while the satellite gives a ratio 1.5; that is to say, according to the model bias calculation, our extrapolation should continue to give an accurate result, while the satellite analysis suggests that we may be overstating the result by 50%. Examination of the results for the two data sets suggests that this is primarily due to a difference in the regions that dominate their speed distributions. For the satellite study, which uses surface data, the highest speeds on the western boundary are in the region where the Gulf Stream is separated from the continent, while for the model study, where the deepest model level was used, the highest velocities are recorded off the coast of South Carolina and Georgia in a region where our measurements are denser. Hence, our extrapolation bias on this boundary is expected to be better represented by the model analysis than by the satellite analysis, accordingly suggesting a bias toward the lower end of this distribution. In the text, however, we conservatively allow for the significant difference implied by the satellite results.

[25] For comparison, the model results estimate WBL dissipation as 33.6 GW and EBL dissipation as 1.4 GW, also highlighting the strong difference on the two boundaries. Satellite results are very different since they measure the much-faster surface currents, and are accordingly not presented.

## 5. Conclusions

[26] Based upon our results, we conclude that BBL dissipation is a major route for the dissipation of subinertial currents in the North Atlantic, with this energy primarily dissipated at shallow depths on the western boundary but also in significant amounts in deeper regions. Losses via this route potentially amount to 40–60% (31–47 GW) of the 80 GW input from wind working on the subinertial surface currents of the North Atlantic. We further estimate that around 40% of the western boundary BBL dissipation occurs in regions with seafloor depth <1 km of the ocean; depths <1 km comprise significantly more than half of measured dissipation in the western boundary. This is consistent with the substantial impact of current velocity on BBL dissipation, $\propto |\mathbf{u}|^3$; mid-ocean Rossby waves are surface-intensified and can thus propagate with little bottom dissipation, but when entering shallower regions, the resulting bottom velocities lead to very high dissipation. This has significant implications for mixing in the North Atlantic; energy dissipated in shallower regions will be unavailable for deep-ocean mixing, leaving the source of the power required to drive these processes ambiguous.

[27] **Acknowledgments.** CJW was funded by a Stratégie d'Attractivité Durable award from the Région Bretagne through the Université de Bretagne Occidental. RBS acknowledges funding provided by NSF grant OCE-0526412 and OCE-0960834, a contract with the National Oceanography Centre, Southampton, UK. BKA was supported by United States National Science Foundation grant OCE-09607820.

## References

Arbic, B. K., J. F. Shriver, P. J. Hogan, H. E. Hurlburt, J. L. McClean, E. J. Metzger, R. B. Scott, A. Sen, O. M. Smedstad, and A. J. Wallcraft (2009), Estimates of bottom flows and bottom boundary layer dissipation of the oceanic general circulation from global high-resolution models, *J. Geophys. Res.*, *114*, C02024, doi:10.1029/2008JC005072.

Bühler, O., and M. E. McIntyre (2005), Wave capture and wave-vortex duality, *J. Fluid Mech.*, *534*, 67–95, doi:10.1017/S0022112005004374.

Chassignet, E. P., H. E. Hurlburt, O. M. Smedstad, G. R. Halliwell, P. J. Hogan, A. J. Wallcraft, R. Baraille, and R. Bleck (2007), The HYCOM (HYbrid Coordinate Ocean Model) data assimilative system, *J. Mar. Syst.*, *65*(1–4), 60–83, doi:10.1016/j.jmarsys.2005.09.016.

Chelton, D. B., M. G. Schlax, R. M. Samelson, and R. A. de Szoeke (2007), Global observations of large oceanic eddies, *Geophys. Res. Lett.*, *34*, L15606, doi:10.1029/2007GL030812.

Ducet, N., P. Y. Le Traon, and G. Reverdin (2000), Global high-resolution mapping of ocean circulation from TOPEX/Poseidon and ERS-1 and -2, *J. Geophys. Res.*, *105*(C8), 19,477–19,498, doi:10.1029/2000JC900063.

Efron, B. (1979), Bootstrap methods: Another look at the jackknife, *Ann. Stat.*, *7*(1), 1–26, doi:10.1214/aos/1176344552.

Ferrari, R., and C. Wunsch (2009), Ocean circulation kinetic energy: Reservoirs, sources, and sinks, *Annu. Rev. Fluid Mech.*, *41*(1), 253–282, doi:10.1146/annurev.fluid.40.111406.102139.

Gill, A. E. (1982), *Atmosphere-Ocean Dynamics*, *Int. Geophys. Ser.*, vol. 30, Academic Press, San Diego, Calif.

Holloway, G., A. T. Nguyen, and Z. Wang (2011), Oceans and ocean models as seen by current meters, *J. Geophys. Res.*, *116*, C00D08, doi:10.1029/2011JC007044.

Hughes, C. W., and C. Wilson (2008), Wind work on the geostrophic circulation: An observational study of the effect of small scales in the wind stress, *J. Geophys. Res.*, *113*, C02016, doi:10.1029/2007JC004371.

Kanzow, T., H. L. Johnson, D. P. Marshall, S. A. Cunningham, Hirschi, A. Mujahid, H. L. Bryden, and W. E. Johns (2009), Basinwide integrated volume transports in an eddy-filled ocean, *J. Phys. Oceanogr.*, *39*(12), 3091–3110, doi:10.1175/2009JPO4185.1.

Molemaker, M. J., J. C. McWilliams, and I. Yavneh (2005), Baroclinic instability and loss of balance, *J. Phys. Oceanogr.*, *35*(9), 1505–1517, doi:10.1175/JPO2770.1.

Munk, W., and C. Wunsch (1998), Abyssal recipes II: Energetics of tidal and wind mixing, *Deep Sea Res. Part I*, *45*(12), 1977–2010, doi:10.1016/S0967-0637(98)00070-3.

Schmitz, W. J., and J. R. Luyten (1991), Spectral time scales for mid-latitude eddies, *J. Mar. Res.*, *49*, 75–107, doi:10.1357/002224091784968585.

Scott, R. B. (1999a), Mechanical energy flux to the surface geostrophic flow using TOPEX/Poseidon data, *Phys. Chem. Earth Part A*, *24*, 399–402.

Scott, R. B. (1999b), Geostrophic energetics and the small viscosity behaviour of an idealized ocean circulation model, PhD dissertation, McGill Univ., Montreal, Que., Canada. [Available from http://www.ig.utexas.edu/people/staff/rscott/.]

Scott, J. R., and J. Marotzke (2002), The location of diapycnal mixing and the meridional overturning circulation, *J. Phys. Oceanogr.*, *32*(12), 3578–3595, doi:10.1175/1520-0485(2002)032%3C3578:TLODMA%3E2.0.CO;2.

Scott, R. B., and Y. Xu (2009), An update on the wind power input to the surface geostrophic flow of the world ocean, *Deep Sea Res. Part I*, *56*(3), 295–304, doi:10.1016/j.dsr.2008.09.010.

Scott, R. B., B. K. Arbic, E. P. Chassignet, A. C. Coward, M. Maltrud, W. J. Merryfield, A. Srinivasan, and A. Varghese (2010), Total kinetic energy in four global eddying ocean circulation models and over 5000 current meter records, *Ocean Modell.*, *32*(3–4), 157–169, doi:10.1016/j.ocemod.2010.01.005.

Scott, R. B., J. A. Goff, A. C. N. Garabato, and A. J. G. Nurser (2011), Global rate and spectral characteristics of internal gravity wave generation by geostrophic flow over topography, *J. Geophys. Res.*, *116*, C09029, doi:10.1029/2011JC007005.

Sen, A., R. B. Scott, and B. K. Arbic (2008), Global energy dissipation rate of deep-ocean low-frequency flows by quadratic bottom boundary layer drag: Computations from current-meter data, *Geophys. Res. Lett.*, *35*, L09606, doi:10.1029/2008GL033407.

Shum, C. K., R. A. Werner, D. T. Sandwell, B. H. Zhang, R. S. Nerem, and B. D. Tapley (1990), Variations of global mesoscale eddy energy observed from Geosat, *J. Geophys. Res.*, *95*(C10), 17,865–17,876, doi:10.1029/JC095iC10p17865.

Weatherly, G. L. (1984), An estimate of bottom frictional dissipation by Gulf Stream fluctuations, *J. Mar. Res.*, *42*, 289–301, doi:10.1357/002224084788502729.

Wunsch, C. (1998), The work done by the wind on the oceanic general circulation, *J. Phys. Oceanogr.*, *28*(11), 2332–2340, doi:10.1175/1520-0485(1998)028%3C2332:TWDBTW%3E2.0.CO;2.

Wunsch, C., and R. Ferrari (2004), Vertical mixing, energy and the general circulation of the oceans, *Annu. Rev. Fluid Mech.*, *36*(1), 281–314, doi:10.1146/annurev.fluid.36.050802.122121.

Zhai, X., and R. J. Greatbatch (2007), Wind work in a model of the northwest Atlantic Ocean, *Geophys. Res. Lett.*, *34*(4), L04606, doi:10.1029/2006GL028907.

Zhai, X., H. L. Johnson, and D. P. Marshall (2010), Significant sink of ocean-eddy energy near western boundaries, *Nat. Geosci.*, *3*(9), 608–612, doi:10.1038/ngeo943.

B. K. Arbic, Department of Geological Sciences, University of Michigan, Ann Arbor, MI 48109, USA. (arbic@umich.edu)

D. F. Furnival, R. B. Scott, and C. J. Wright, Laboratoire de Physique des Océans, Université de Bretagne Occidental, Brest F-29200, France. (darran.furnival@univ-brest.fr; robert.scott@univ-brest.fr; corwin.wright@univ-brest.fr)